International Journal of Design & Nature and Ecodynamics
Vol. 20, No. 3, March, 2025, pp. 501-514
Journal homepage: http://iieta.org/journals/ijdne

Carbonized Bamboo Culm-Based Composite Materials: Mechanical and Frictional Performance for Brake Pad Applications

Ishaya Musa Dagwa[1], Ogochukwu Eugenia Okeke[1], Musa Tanko Zarmai[1], Ibrahim Momoh-Bello Omiogbemi[2], Adekunle Akanni Adeleke[3], Peter Pelumi Ikubanni[4], Emmanuel Omotosho[5*]

[1] Mechanical Engineering Department, University of Abuja, Abuja 900001 Nigeria
[2] Mechanical Engineering Department, Air Force Institute of Technology, Kaduna 800283, Nigeria
[3] Department of Mechanical Engineering, Nile University of Nigeria, Abuja 900001 Nigeria
[4] Department of Mechatronics Engineering, Bowen University, Iwo 232101 Nigeria
[5] Department of Finance, Durham University, Durham DH1 3LB, UK

Corresponding Author Email: emmanuel.o.omotosho@durham.ac.uk

https://doi.org/10.18280/ijdne.200305

Received: 26 February 2025
Revised: 18 March 2025
Accepted: 25 March 2025
Available online: 31 March 2025

Keywords:
carbonization, bamboo culm, composite, mechanical properties, TGA, SEM

ABSTRACT

This study examines the development and application of composite materials based on dry and carbonized bamboo culm particles for friction material applications, particularly as a potential replacement for asbestos-based materials. Due to the environmental and health risks associated with asbestos, sustainable, high-performance alternatives are essential. Carbonized bamboo particles offer excellent thermal stability, while bamboo culm enhances strength. The development involved selecting bamboo culm composites, carbonizing, drying, and integrating them with other materials to achieve the desired friction properties. The composite materials were developed in a laboratory setting, and mechanical and thermal experiments were used to characterize the materials' properties. A systematic experimental design approach, including the Taguchi method, was employed to optimize the formulation and processing parameters. Test results show that the developed composite material has high mechanical strength, with an average tensile strength of 10.31 ± 0.21 MPa, a modulus of elasticity of 80.07 ± 1.60 MPa, an impact strength of 0.6912 J/mm, and a Vickers hardness of 107 HV. Thermal stability was further confirmed during testing, with a maximum temperature of 950°C at a heating rate of 10°C/min. The developed composite material also performed well in friction material tests, with a friction coefficient of 0.378 and a wear rate of 0.15 mm³/Nm. Thermogravimetric analysis showed that optimized carbonized bamboo brake pads had lower temperature degradation than commercial ones. Results indicated that dry and carbonized bamboo culm composite materials are effective for friction applications, performing comparably to commercial brake pads.

1. INTRODUCTION

Automobile brakes are essential for controlling vehicle speed by converting kinetic energy into heat, which is primarily dissipated into the atmosphere [1-3]. However, the use of asbestos fibers in brake pad manufacturing has raised significant health and safety concerns due to their carcinogenic properties. Although asbestos was favored in brake pads for its sound absorption, moderate tensile strength, and heat resistance, it has been recognized as a carcinogen since the 1970s linked to severe health issues such as malignant lung cancer, mesothelioma, and asbestosis (an interstitial lung disease caused by inhalation of asbestos fibers). Although the U.S. Environmental Protection Agency (EPA) banned asbestos in brake pads in March 2024, risks remain for those exposed to older brake pads containing asbestos, highlighting the need for continued awareness and research into safer alternatives [2, 4-6]. To address these concerns, researchers have explored alternative materials such as metals, ceramics, carbon, and organic composites for brake pad production [7]. Natural fibers, particularly agricultural waste, have been increasingly utilized as sustainable replacements for asbestos fibers [8]. Ibhadode and Dagwa [7] developed asbestos-free friction lining materials from palm kernel shells, which performed satisfactorily compared to commercial asbestos-based brake pads. Similarly, Ruzaidi et al. [9] investigated palm slag-based brake pads, demonstrating their effectiveness as a friction material. Other studies have explored combinations of coconut fiber and palm kernel shell [10, 11], kenaf fibers [12], and bagasse [13] as potential replacements for asbestos.

Bamboo culm, a lignocellulose biomass, presents a promising alternative due to its rapid growth rate, high mechanical strength, and organized fiber distribution. Its primary chemical components—cellulose, hemicellulose, and lignin—contribute to its structural integrity [14-16]. Azeez

and Orege [14] found that the chemical composition of bamboo fibers varies with age, while Vivas [15] linked bamboo's mechanical properties to factors such as species, density, and moisture content. Yunhai et al. [16] demonstrated that carbonized bamboo fibers enhance friction material performance by reducing noise and retaining wear debris.

Brake pads are composed of several key materials that work together to ensure effective braking performance [17, 18]. These include binding components, or binders, which hold the other materials together; abrasive components that create friction against the brake rotor; and performance components such as temperature-specific lubricants that enhance braking efficiency. Additionally, filler materials are added to improve specific properties, while structural materials help maintain the pad's shape during operation. The precise formulation of these components is crucial for optimizing braking characteristics [17-22]. Figure 1 illustrates the transformation process from fresh bamboo culm to carbonized bamboo culm. While various bio-based materials have been explored in brake pad production, the potential of bamboo ash (BA) remains under-researched, presenting an opportunity for further investigation into its applications in friction materials.

As previously discussed, asbestos-based friction materials have long been used in brake pad production but were later identified as carcinogenic, prompting widespread concern and subsequent research into safer alternatives [23, 24]. This study investigates the potential of locally sourced bamboo culm as a sustainable and eco-friendly base material for brake pad production, providing an alternative to carcinogenic asbestos fibers. This research adopts an innovative approach by combining carbonized bamboo culm with additives such as epoxy resin, cast iron filings, graphite, and aluminum oxide to create a composite brake pad. The objectives of this study are: (i) to process and optimize bamboo culm for friction material applications, (ii) to fabricate a composite brake pad using carbonized bamboo, (iii) to evaluate its mechanical and tribological properties, including wear rate, hardness, and friction coefficient, and (iv) to compare its performance against commercial brake pads. By focusing on bamboo culm as a renewable resource, this study contributes to sustainable material development while addressing health and environmental concerns associated with asbestos use.

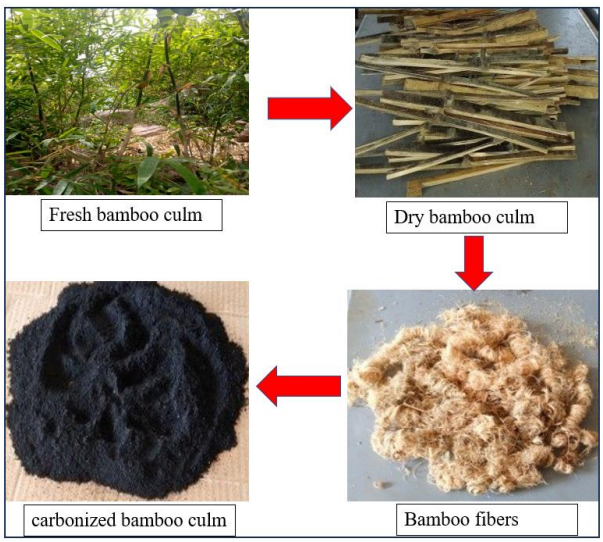

Figure 1. Material transformations (a) fresh bamboo culm, (b) dry cut bamboo culm, (c) bamboo fibres, and (d) carbonized bamboo culm

2. MATERIALS AND METHODS

2.1 Materials

The materials utilized in this study include bamboo culm, epoxy resin (Epochem 205: Bisphenol-A-glycidyl ether), hardener (Epochem 105: Triethylenetetramine), graphite, aluminum oxide, and cast-iron filings, all sourced from a chemical shop in Zaria, Nigeria. The bamboo culm was harvested from a swampy riverside area in Sun-City, Abuja, where bamboo trees grow abundantly in the wild.

2.2 Experimental procedure

The sample of brake pads produced in this research work was carefully done according to Lobovikov et al. [25], following the standard procedure as described by Azeez and Orege [14] and Deng [26], evaluated with the standard test method adopted by Vivas [15]. The following methods were adopted during this research work: processing of the material composites and property determination of the prepared samples.

2.2.1 Processing of the bamboo culm

Three dozen bamboo culms, each length 100 mm, were collected and sun-dried for three weeks to remove the moisture contents from 48% to 15%, after which it was cut into smaller sizes using a hand saw. The bamboo culm was ground into a powdery form using a grinding machine (Model: Black & Decker CDJ15) and then sieved with various sieve sizes of 75, 150, and 212 microns to get the fine powder that was used for the experimental analysis. The ground-based material was divided into two parts; one part was carbonized, and the other part was left uncarbonized. The first part was carbonized using a muffle furnace at different temperatures (400, 500, 700, and 800°C) and time. The effect of carbonization temperature (400, 500, 700, and 800°C) on the mechanical properties of the bamboo-based composite shows a progressive improvement up to an optimal point. As temperature rises, notable enhancements in hardness, density, and wear resistance occur due to increased carbon content and structural transformation [27-29]. Figure 2 depicts the flow chart of the carbonization process from inception to completion.

2.2.2 Formulations of the hybrid

Table 1 shows various compositions of carbonized and un-carbonized base materials that were used in determining the effects of different particle sizes of the ground base material. The experiment was conducted by measuring and weighing all the materials used in the right proportion using the standard rule of mixture which agrees with what researchers have reported in previous literature [8, 30, 31], 30 ml of epoxy resin and 15 ml of hardener was poured into a container and thoroughly stirred for about 2 minutes. Thereafter, the other additives (Graphite, Aluminum oxide, and Cast-iron fillings) were poured consecutively into the earlier mixture of epoxy resin with a hardener and stirred for another 3 minutes to obtain a homogenous mixture. The mixture was further poured into a fabricated mold of 5 mm, which had been covered with paper foil, which was then put into a compression molding machine at a temperature of 130°C and pressure of 2.5 MPa and allowed to cure for 5 minutes. Thereafter, it was allowed to cool for 2 minutes and then removed from the mold and weighed. This process was repeated for all the carbonized and

un-carbonized samples. The samples were cut to different standard dimensions for various analyses. The 2.5 MPa pressure was used to avoid air traps on the composite material, as well as for compaction purposes. Based on some previous works by researchers [7, 13, 32, 33], trial formulations were carried out using 75, 150, and 212 µm particle sizes of bamboo culm base material to ascertain the optimal particle size.

The molding parameters (temperature, pressure, time, and heat treatment) were optimized using the Taguchi $L_9(3)^4$ orthogonal array method of experimental design. The method comprises 4 factors (molding parameters) with 3 levels each, as indicated in Table 2. The orthogonal array for these parameters can be seen in Table 3.

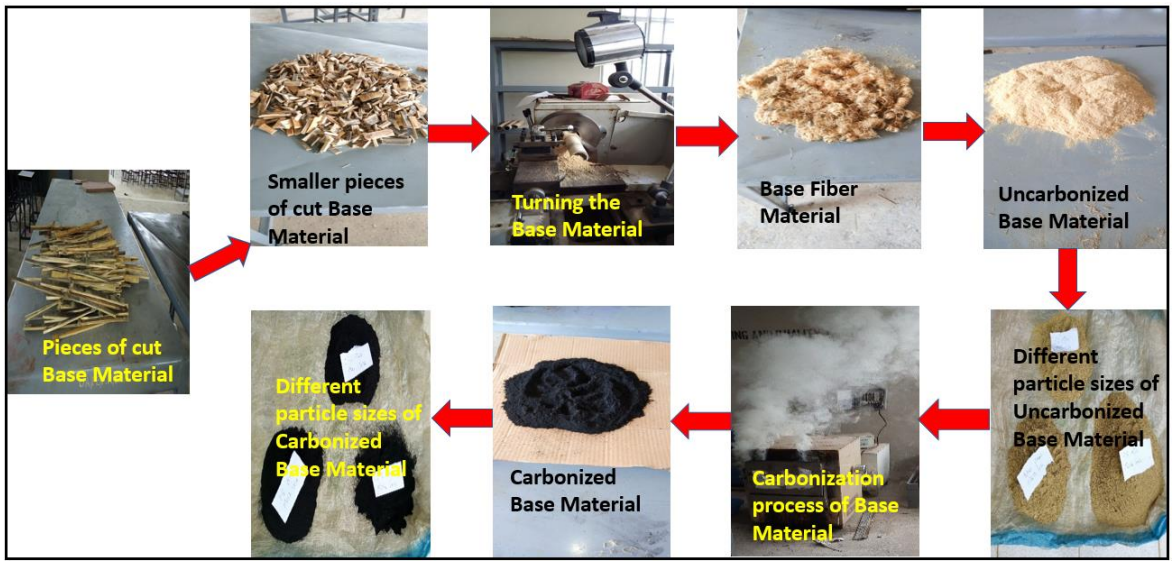

Figure 2. Flow chart of the carbonization process

Table 1. Different particle size formulations

	Materials	Carbonized Particle Sizes			Un-Carbonized Particle Sizes		
		75 µm	150 µm	212 µm	75 µm	150 µm	212 µm
		A1	A2	A3	A1	A2	A3
1	Epoxy Resin	30	30	30	30	30	30
2	Hardener	15	15	15	15	15	15
3	Base Material	40	40	40	40	40	40
4	Graphite	5	5	5	5	5	5
5	Aluminium Oxide	5	5	5	5	5	5
6	Cast Iron Fillings	5	5	5	5	5	5
	TOTAL	**100**	**100**	**100**	**100**	**100**	**100**
		B1	B2	B3	B1	B2	B3
1	Epoxy Resin	30	30	30	30	30	30
2	Hardener	15	15	15	15	15	15
3	Base Material	35	35	35	35	35	35
4	Graphite	5	5	5	5	5	5
5	Aluminium Oxide	10	10	10	10	10	10
6	Cast Iron Fillings	5	5	5	5	5	5
	TOTAL	**100**	**100**	**100**	**100**	**100**	**100**
		C1	C2	C3	C1	C2	C3
1	Epoxy Resin	30	30	30	30	30	30
2	Hardener	15	15	15	15	15	15
3	Base Material	30	30	30	30	30	30
4	Graphite	10	10	10	10	10	10
5	Aluminium Oxide	5	5	5	5	5	5
6	Cast Iron Fillings	10	10	10	10	10	10
	TOTAL	**100**	**100**	**100**	**100**	**100**	**100**

Table 2. Molding parameters and levels

S/N	Factors	Levels		
		1	2	3
1	Molding Temperature (°C)	125	135	145
2	Molding Pressure (MPa)	2.0	2.5	3.0
3	Molding Time (Min)	4.0	6.0	8.0
4	Heat Treatment (h)	1.0	3.0	5.0

2.3 Research characterization and optimization of brake pad samples

To determine the elemental compositions of carbonized and uncarbonized composites, samples were prepared and analyzed using Energy Dispersive X-ray Fluorescence (EDXRF) spectroscopy. This technique provides qualitative and quantitative data on elemental constituents, including

major oxides like SiO_2. The EDXRF spectra are acquired and analyzed to identify peaks that indicate specific elements and their concentrations. Findings are documented in tables and figures to clearly present the elemental compositions of the composites.

To obtain the empirical values of the important analytical brake pad properties, standard tests were performed on each set of samples.

Table 3. Orthogonal array for the molding parameters

Experimental Run	Moulding Parameters			
	Molding Temperature (ºC)	Molding Pressure (MPa)	Molding Time (min)	Heat Treatment (Annealing) (h)
T1	125	2.0	4.0	1.0
T2	125	2.5	6.0	3.0
T3	125	3.0	8.0	5.0
T4	135	2.0	6.0	5.0
T5	135	2.5	8.0	1.0
T6	135	3.0	4.0	3.0
T7	145	2.0	8.0	3.0
T8	145	2.5	4.0	5.0
T9	145	3.0	6.0	1.0

2.3.1 Density determination

According to Naik et al. [34], the mass of the samples was analyzed to an accuracy of ±0.2 g to determine the composites' density using the ASTM D792-20 standards [35]. Each sample was weighed on a computerized scale to obtain the various masses (m), which were then used to calculate the densities of each sample. The average was calculated after this experiment was run in triplicate per sample. Eq. (1) was used to evaluate the density of the composites.

$$\text{Density } (\rho) = \left[\frac{M\ (g)}{V\ (cm^3)}\right] \quad (1)$$

where, M = mass of sample (g) and V = volume of sample (cm^3).

2.3.2 Water absorption test

A testing procedure used to verify the moisture content of the produced hybridized composite as a proportion of its dry weight is called the water absorption analysis. This test was carried out in accordance with ASTM D570, which Edokpia et al. [33] and Nishino et al. [36] adopted, using a rectangular sample of dimension (50 × 50 × 5 mm) acquired from the developed composite samples. To remove any potential moisture, the samples were dried in an oven at 50°C for 24 hours [37]. For 24 hours, the samples were completely submerged in distilled solution at 25°C (77°F). After that, they were taken out, dried with filter paper, and weighed once more with a digital scale (Model: BL20001). In this instance, the percentage water absorption (WA) formula from Eq. (2) was used to evaluate the water absorption utilizing the material's weight gain approach.

$$\text{WA} = \left[\frac{W2-W1}{W1}\right] \times 100 \quad (2)$$

where, W1 is the dry weight and W2 is the wet weight of samples.

2.3.3 Oil absorption test

The oil absorption test was conducted by prior weighing each composite sample on a digital weighing balance. Afterward, the samples were immersed separately in SAE60 automotive engine oil at time intervals of 24 hours. The composite samples were removed from the oil, cleaned using a dry cloth, and re-weighed. The difference in weight between the initial and final weight was calculated and recorded, as well as used to determine the absorption rate as posited by Edokpia et al. [33]. The weight measurements were taken periodically at time intervals of 24 hours for the whole sample. The percentage of oil absorption of the composites was calculated using Eq. (3) as adopted by Smales [38];

$$\text{OA} = OA_1 - \left[\frac{OA_0}{OA_0} \times 100\right] \quad (3)$$

where, OA (%) is the percentage of oil absorption, OA_0 is the initial weight of the composite before immersion, and OA_1 is the final weight of the composite after immersion. The oil absorption result for the carbonized composite materials was recorded and tabulated which was used to ascertain the diffusion mechanism. Figure 3(a) and (b) shows the absorption test samples soaked in distilled water and SAE60 automotive oil, respectively.

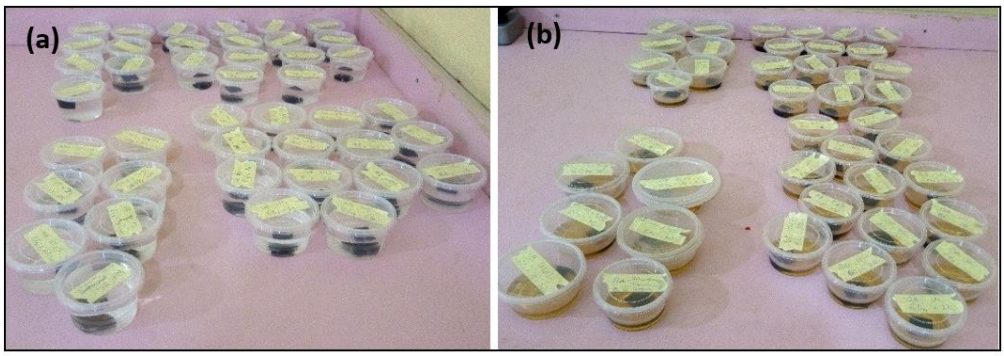

Figure 3. Absorption test samples soaked in (a) distilled water and (b) SAE60 automotive oil

2.3.4 Hardness test

To determine the hardness values of the composites, the Vickers hardness testing machine (Model MV1-PC) was used in accordance with the ASTM D-2240 standard as reported by some researchers [30, 31]. Three sections of surfaces of each sample of the composite with dimensions of 30 mm, 30 mm, and 5 mm were subjected to Vickers hardness tests, and an average was recorded.

2.3.5 Tensile test

The Hounsfield Monsanto Tensometer (Model: 386083-W9), operating at a cross speed of 10 mm/min, was used to conduct the tensile test in accordance with the ASTM D-638-03 standards adopted by some researchers [30, 31, 39]. A tensile force and tensile properties, such as tensile strength, were applied to the samples cut to standard for experimentation with the dimensions as shown in Figure 4. This test was done on the produced and commercially available samples.

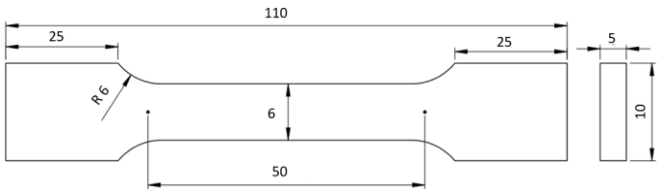

Figure 4. The sample set up for tensile analysis (all measurements in mm)

2.3.6 Impact test

The impact test was conducted using the Izod impact testing machine (Model 4123-07-15269C) with a maximum capacity of 15 kg-m (150 J). The test sample of dimension (80 × 20 × 5) mm having a notch angle of 40° with a 2 mm notch depth and a notch radius of 0.25 mm was mounted on the impact testing machine while the pendulum was released to calibrate the sample which was horizontally gripped in a vice with the required force applied from the swinging pendulum to break the bar. The experiment was conducted three times for the samples with various readings obtained and recorded accordingly [39]. This test was conducted on both the produced and commercially available samples.

2.3.7 Compression test

The test was carried out to determine the behavior of the material as it experiences a compressive load. The rectangular-shaped sample used was gripped to the universal testing machine (Model: Cat. Nr. 261) with 100 kN capacity, and a load was applied with strain recorded at intervals. The samples for brake pad development were subjected to compressive force continuously until failure occurred, and the load at which failure occurred was recorded [13]. This test was carried out on both the samples produced internally and those obtained from commercial sources.

2.3.8 Thermogravimetry test

Thermogravimetric analysis (TGA) is an indispensable method that is mostly used in materials science and engineering to analyze the thermal stability of natural and other kinds of fibers. TGA can assess the quantity and intensity of weight variations as a function of temperature or time in a wide range of controlled environments. Thermal stability may typically be predicted using TGA results within a temperature range of up to 1000°C [30, 40]. Utilizing Perkin Elmer's thermal analysis (Model: TGA 4000), TGA was used to determine the thermal stability of the composite in a nitrogen environment with a heating rate of 10°C/min. The samples were heated at a temperature range of 30°C to 950°C.

2.3.9 Wear test

A ball-on-disc tribometer testing machine (Model: 20-8054 Graz-Austria) was used for the wear test analysis. The sample used for the experiment was held against the counter face of the rotating disc with a wear track radius of 5 mm, and the test was conducted under a load of 5 N. Each sample of wear resistance had a 110 mm diameter and a 5 mm thickness. Before the test, each sample was weighed and recorded using a BL20001 4-digit electronic weighing scale. With the help of a nut in the center, the sample was secured to a machine's 100 mm-diameter rotating disc. The sample affixed to the rotating disc was permitted to come into direct touch with two emery wheels located on the machine's top arm. According to Ademoh and Olabisi [41], the machine was powered by a 220 V, and the disc revolved at a steady speed of 85 r.p.m. for a pre-set time of 1000 seconds. The two emery wheels in close proximity to the specimen rotated in tandem with the disc as it spun, wearing down the sample as a result. The equipment automatically shuts off after the predetermined period. The item was meticulously cleaned, and the final weight was measured and noted. Eq. (4) [41] was used to calculate the wear rate from the specimen's weight loss using the difference between the final and initial weights.

$$\text{Wear Rate} = \frac{W0-W1}{S} = \frac{\Delta W}{S} = \frac{\Delta W}{2\pi ND \times t} \quad (4)$$

where, W_0 represents the starting weight, W_1 represents the end weight, ΔW represents the weight loss, S represents the sliding distance (mm), D represents the disc diameter (mm), N represents the radial speed (rpm), and t represents the exposure time (s) for the sample to wear.

2.3.10 Coefficient of friction test

The coefficient of friction test was conducted using an inclined plane apparatus (Model: SKU PH0334). Each sample was set up as shown in Figure 5 on an inclined plane with a specified inclination and a 90° wedge. To increase the angle, the wedge location was changed until the specimen was about to slip down the plane. The resultant coefficient of static friction (μ) was calculated using Eq. (5) [41].

$$\mu = \tan\theta = \frac{\text{Opposite}}{\text{Adjacent}} \quad (5)$$

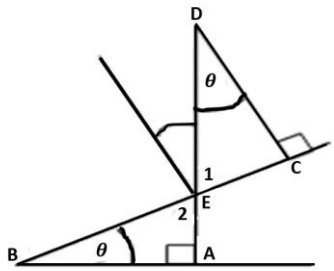

Figure 5. Illustration of sample for the coefficient of static friction examination

2.3.11 X-ray diffraction (XRD) test

Phase characterization of the carbonized produced sample was performed using X-ray diffraction (XRD) on a Rigaku MiniFlex 600-C diffractometer, equipped with Cu-Kα radiation (wavelength 1.5406 Å), operating at 40 kV and 15 mA. To eliminate background interference, the analysis was conducted using a single-crystal quartz holder. The XRD scan was executed with a scan speed of 2°/min, covering a 2θ range of 2°–70°, with 0.02° increments in a locked coupled configuration adopting Sá Ribeiro et al. [42] and Chin et al. [43] methods.

2.3.12 Scanning electron microscope (SEM) test

SEM (Model: PW-100-012) microstructural analysis of the composite samples was performed to investigate the type of interfacial bonding that exists in the composite. To ensure excellent conductivity of the samples mounted on the stubs with a silver plate of the SEM machine, the surface of the samples for analysis was initially prepared by a vacuum-evaporation mechanism of a thin platinum film. Thereafter, the micrographs were taken seamlessly [44].

3. RESULTS AND DISCUSSION

The elemental compositions of carbonized and uncarbonized composites are given in Table 4. The major oxide in the material, SiO_2, has a hexagonal crystal structure and makes up roughly 12.91 wt.% of it, as shown in Table 4. However, Table 4's validation of the trigonal hematite crystal structure shows that it has a high degree of crystallinity. Due to its advantageous characteristics, including hardness, silicon oxide plays a crucial role in the manufacture of brake pads. According to Table 4, the hexagonal structure of SiO_2 is approximately 1.939 wt.%, with a low crystallinity trigonal hematite crystal structure [45]. Al_2O_3, present at 2.266 wt.% in the carbonized composite sample and 0.416 wt.% in the uncarbonized composite sample, is renowned for its exceptional hardness and thermal resistance. This oxide plays a crucial role in significantly enhancing the wear resistance of the composite material [45, 46]. Potassium oxide (K_2O), widely used as a flux in ceramic applications, effectively reduces the melting point of silica, thereby enhancing the workability of the composite material. Iron (III) oxide (Fe_2O_3) and magnesium oxide (MgO), as basic oxides, make significant contributions to the mechanical properties and thermal stability of the carbonized composite. Phosphorus pentoxide (P_2O_5), recognized for its strong dehydrating properties, enhances the durability of the composite by promoting cross-linking during the curing process. Additionally, calcium oxide (CaO), or quicklime, is vital for improving both the mechanical strength and overall durability of the composite material [45-48]. The analysis indicates that the carbonized base material exhibits superior performance compared to the uncarbonized base material, as shown in Table 4.

Table 4. Compositions of carbonized and uncarbonized base material

Oxide Composition of Carbonized Base Material													
Element/Oxides	Fe_2O_3	SiO_2	Al_2O_3	MgO	P_2O_5	SO_3	TiO_2	MnO	CaO	K_2O	CaO_2	ZnO	CuO
Weight (wt.%)	3.634	12.91	2.266	1.340	1.330	0.341	0.141	0.213	2.145	7.083	1.110	0.061	0.022
Oxide Composition of Uncarbonized Base Material													
Element/Oxides	Fe_2O_3	SiO_2	Al_2O_3	MgO	P_2O_5	SO_3	TiO_2	MnO	CaO	K_2O	CaO_2	ZnO	CuO
Weight (wt.%)	1.014	1.939	0.416	0.040	0.990	0.218	0.028	0.101	0.531	1.650	0.039	0.033	0.013

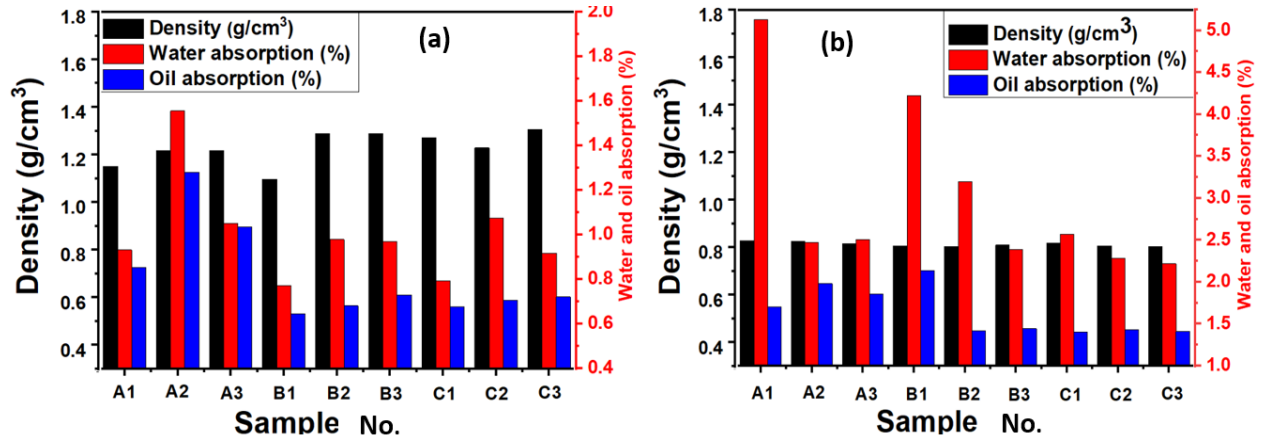

Figure 6. Effects of particle sizes on density, water absorption, and oil absorption of (a) carbonized base material and (b) uncarbonized base material

3.1 Effects of particle sizes on the physical properties of the Composites

Figure 6(a) and 6(b) presents the results of tests conducted to evaluate the effects of different particle sizes of carbonized and uncarbonized base materials. The analysis includes density, water absorption, and oil absorption tests, which are critical for assessing the suitability of these materials for various applications [49]. In the figures, A1, B1, and C1 represent a particle size of 75 µm, while A2, B2, and C2 correspond to 150 µm, and A3, B3, and C3 indicate 212 µm. These classifications are further supported by data in Table 1. Upon comparing the outcomes illustrated in Figures 6(a) and 6(b), it was noted that sample B1 (75 µm) of the carbonized base material exhibited the lowest density at 1.1 g/cm³. Additionally, it demonstrated a water absorption rate of 0.768

and an oil absorption rate of 0.645, both of which were lower than those of the other samples tested. These findings highlight the superior performance characteristics of the 75 µm particle size. The study indicates that smaller particle sizes, particularly 75 µm, improve the mechanical properties of composites, including lower density and water and oil absorption. This implies that fine particles enhance interfacial bonding, promoting better material integrity and load transfer in the composite matrix. Consequently, this necessitated the selection of 75 µm as the optimal particle size for further investigation, guiding the development of composite materials with enhanced properties for practical applications [50, 51].

3.2 Hardness characterization for carbonized and uncarbonized base materials

Figure 7 presents the results of Vickers hardness characterization for carbonized and uncarbonized base material samples. It was seen from the results that the carbonized base material of sample No. 3 gave the highest hardness property (91.7 ± 2.75 HV) compared to the other carbonized and un-carbonized base material samples at the preliminary test. This performance was due to the increase in the bonding materials in the composition of sample No. 3 (epoxy resin and carbonized grounded bamboo culm) as well as the close packing that strain-hardened the composite brake pad and raised its hardness properties compared to other compositions. Due to the bond interaction of epoxy, which keeps the components together, the hardness value increased as reinforcement levels increased. The result is in consonant with the works of some researchers on brake pad application [15, 16]. At this stage, the sample No. 3 composition of carbonized samples was further used to carry out the next stage of experimentation using Taguchi experimental run (L9) method and the resultant hardness values (Samples R1-R9) and the control sample R10 are illustrated in Figure 7(b) while the uncarbonized base material was not considered for further specimen production. It can be observed also that from the outcome of the hardness test analysis (Figure 7(b)) from the Taguchi experimental run (L9) samples that sample R9 gave the highest hardness values (109.3 ± 2.73 HV) as compared to other samples R1, R2, R3, R4, R5, R6, R7, R8 and R10 with hardness values of 69.5 ± 1.34 HV, 81.7 ± 2.04 HV, 79.2 ± 1.91 HV, 90.8 ± 2.27 HV, 95.7 ± 2. 39 HV, 101.7 ± 2.54 HV, 104.7 ± 2.62 HV, 102.7 ± 2.57 HV, and 67.3 ± 1.68 HV, respectively. This showed that the control sample R10 gave the least hardness properties. It can be evident that sample R9 possesses toughened characteristics with the capacity to withstand indentation as viewed by Dagwa et al. [30] and Mohamed et al. [52]. The results obtained generally compared favourably with those of conventional brake pad (101 HV) as posited by Ademoh and Olabisis [41].

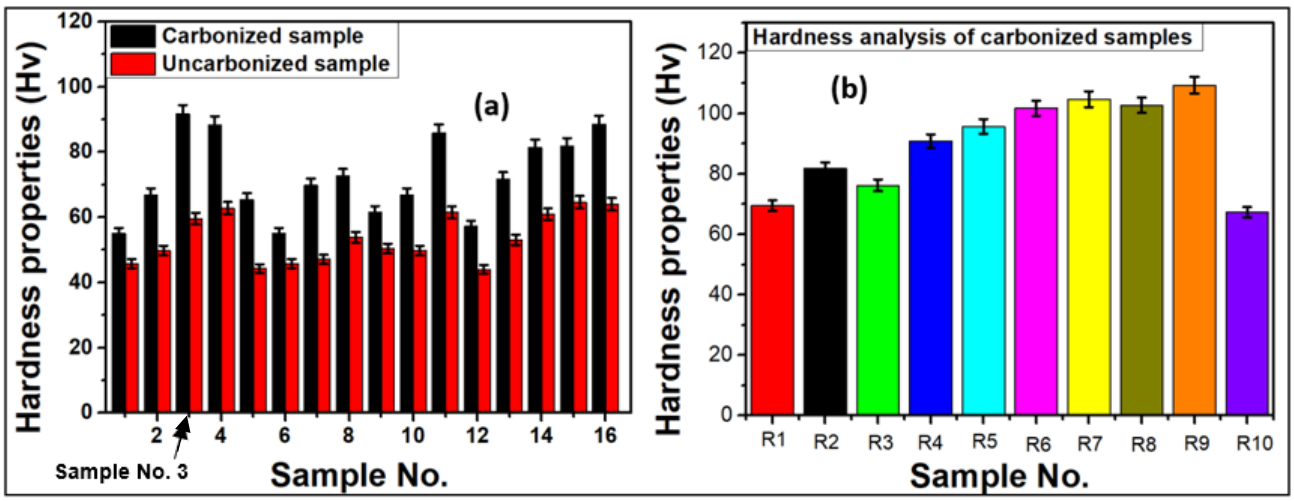

Figure 7. Hardness characterisation for carbonized and uncarbonized samples

Table 5. Tensile test results

S/N	Samples	Average Breaking Load (N)	Average Extension (mm)	Tensile Strength (MPa)	Strain	Modulus of Rupture (MPa)
1	Produced	396.00 ± 7.92	6.44	10.31 ± 0.21	0.1288	80.07 ± 1.60
2	Commercial	485.00 ± 9.70	5.10	12.63 ± 0.25	0.1020	123.83 ± 2.48

3.3 Tensile analysis

Table 5 presents the tensile test results for the developed brake pad sample alongside a commercially obtained brake pad. The tensile strength of the developed sample was measured at 10.31 ± 0.21 MPa, with a modulus of rupture of 80.07 ± 1.60 MPa. In comparison, the commercial brake pad exhibited a higher tensile strength of 12.63 ± 0.25 MPa and a modulus of rupture of 123.83 ± 2.48 MPa. Despite this, the tensile strength of the developed brake pad falls well within the range reported for conventional brake pads, such as 7.00 MPa [41], and aligns closely with the performance of other developed brake pads [53, 54]. These findings suggest that the developed brake pad exhibits competitive and acceptable mechanical properties, making it a viable alternative to conventional and commercial brake pads.

3.4 Impact analysis

Figure 8 illustrates the impact energy results for both the developed and commercial brake pad samples. The developed brake pad exhibited an impact energy of 0.691 ± 0.013 J/mm,

closely matching the commercial sample's 0.716 ± 0.014 J/mm, which was used as a control. Notably, the impact energy of the produced sample falls within the recommended range for brake pad applications, such as 0.082 J/mm, as highlighted by Abutu et al. [53]. The commendable impact energy of the developed sample can be attributed to the inclusion of cast iron filings as reinforcement, which significantly enhances its energy absorption capability. This favorable comparison demonstrates the efficacy of the produced brake pad in maintaining mechanical integrity under impact, highlighting its potential as a reliable and competitive alternative for braking system applications [55, 56].

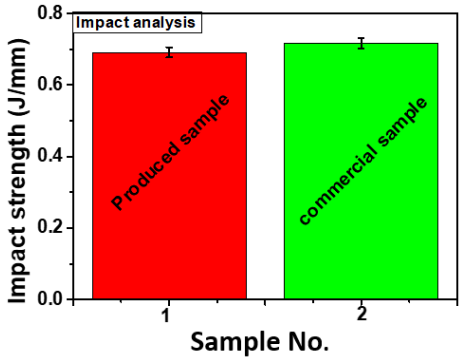

Figure 8. Impact analysis of produced and commercial samples

3.5 Compression analysis

Table 6 presents the results of the compression test conducted on three samples each of the developed and commercial brake pads, with their averages and standard deviations recorded. The analysis reveals that the developed brake pads reinforced with bamboo culm demonstrated superior performance, achieving an average compression strength of 13.747 ± 0.412 MPa. This performance is notably higher than that of the commercially available brake pads, which recorded a similar average compression strength. Furthermore, the results align well with the findings of previous studies, such as those by study [57], which investigated brake pads developed using coconut shell reinforcement materials, reporting minimum compression strengths ranging from 3.817 to 5.451 MPa. The enhanced compression strength of the developed brake pads indicates their robustness and suitability for reliable braking system applications.

Table 6. Compression strength results for produced and commercial samples

Sample Type	Average Thickness (mm)	Average Width (mm)	Average Compression Strength (kN)
Produced sample	8.467 ± 0.254	19.067 ± 0.572	13.747 ± 0.412
Commercial sample	9.933 ± 0.297	15.933 ± 0.478	6.450 ± 0.194

3.6 Thermogravimetry analysis

Figure 9(a) and (b) show the curve of TGA (changes in weight % to the corresponding temperature) of the produced composite sample (bamboo culm, cast iron fillings, alumina, and epoxy) and its first derivatives (DTG) and the commercial composite sample (control sample) respectively that show the temperatures of optimum decomposition. As evident from Figure 9(a) and (b) respectively, the produced composite material was stable up to about 319°C and started degrading from a temperature of 320°C until it became rapid at 580°C while the commercial sample was stable up to about 291°C and started degrading from a temperature of 292°C until it became rapid at 550°C which is closely related to the average degradation temperature of fiber-related brake pad materials [30, 58]. It is evident that the produced composite materials experienced lower temperature degradation as compared to their counterpart commercial sample of brake pad used as control. These findings are corroborated by the works of Dagwa et al. [30], Yao et al. [58], and Kozłowski and Przybylak [59] on the degradation characteristics of composite materials for different engineering applications.

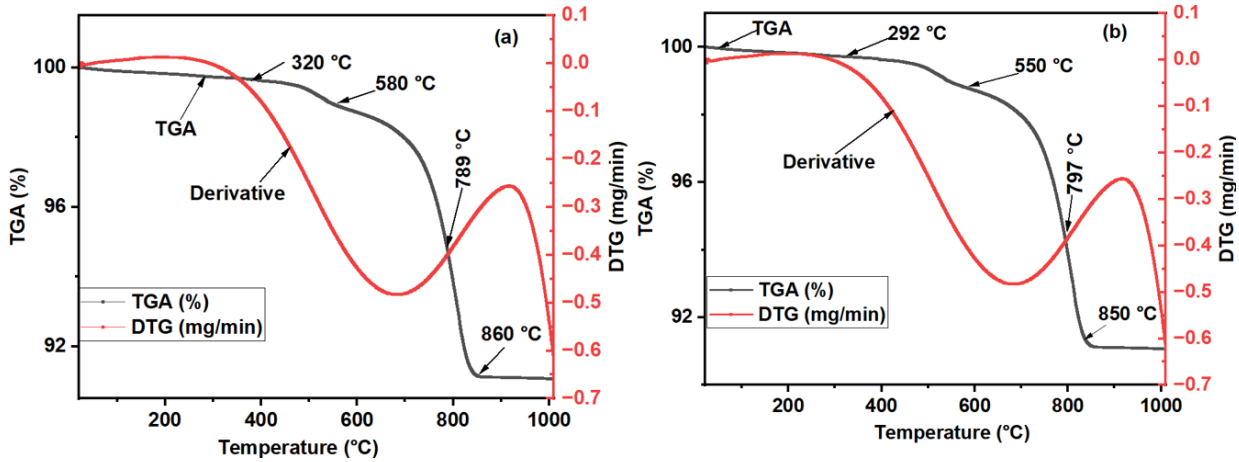

Figure 9. TGA/DTG graph of (a) the produced composite sample brake pad and (b) the commercial sample brake pad

3.7 Effect of sample weight, coefficient of friction, and wear rate characterizations

Figures 10(a) and (b) present the wear rate characterizations of the produced sample of the brake pad. It is evident that the values of the wear rate decrease with the increased coefficient of friction of the samples (Figure 10(b)), while sample weight maintains relatively uniform values (Figure 10(a)). This can be attributed to the high hardness properties and compressive strength of the developed composite samples of brake pads,

which slightly differ from the commercial brake pad sample [13]. Conversely, the obtained coefficient of friction values of the developed samples of brake pads and commercial samples (Figure 10(a) and (b)) fall within the standard range of 0.3-0.4 [41, 60]. Therefore, the coefficient of friction of the developed sample brake pad compares favourably with that of a conventional brake pad obtained from a standard [41]. In contrast, the friction coefficients of the composite samples 1, 4, 5, 6, 7, 8, and 9 ranged by 20.64, 21.22, 18.90, 15.41, 18.02, 22.09, and 20.06%, respectively, above the mean values of those of commercial brake pads (0.344). With variances of 0.02 µ, 0.06 µ, and 0.14 µ, respectively, the friction coefficient of sample 6 composition (0.173 µ) was higher than that of related works by Aigbodion et al. [13] that used bagasse filler, Yawas et al. [32] that used periwinkle filler, and Edokpia et al. [33] that used eggshell filler for composite brake pads. It also competed favorably with the works of Ibhadode and Dagwa [7], which used conventional filler with a variation of 0.09 µ. However, it is corroborated by the value (0.44) obtained by Dagwa and Ibhadode [60]. The wear rate of the composite brake pad composition 6 differed from that of the commercial brake pad by 0.010, making composite 6 a superior brake pad material to the conventional brake pad. In comparison with previous works, composition 6 was better than the brake pad made with conventional material [7], bagasse filler [13], periwinkle filler [32] and eggshell filler [33].

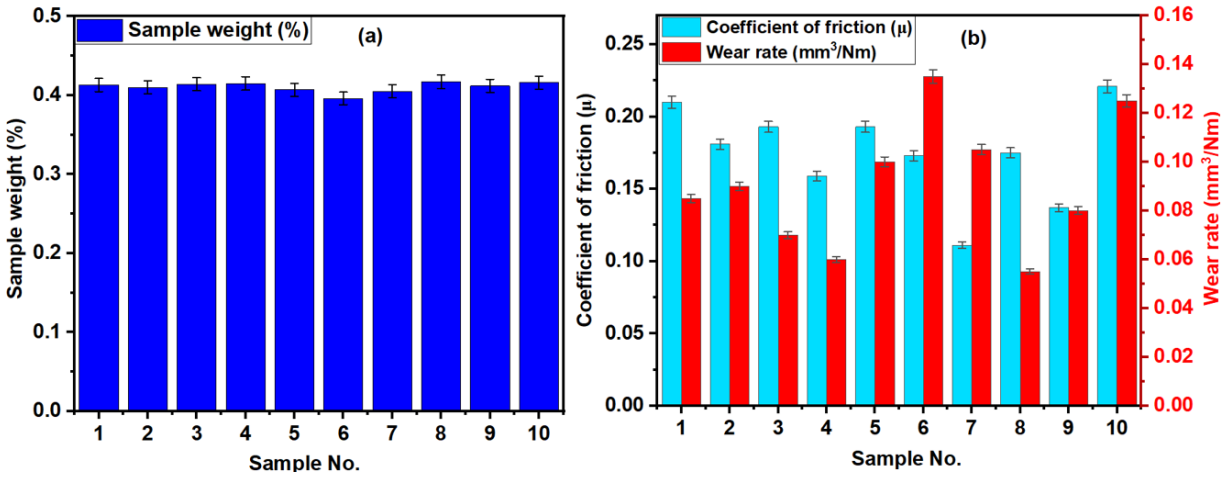

Figure 10. Wear rate properties of the developed sample brake pad material (a) sample weight and (b) comparison of coefficient of friction vs wear rate

3.8 XRD analysis

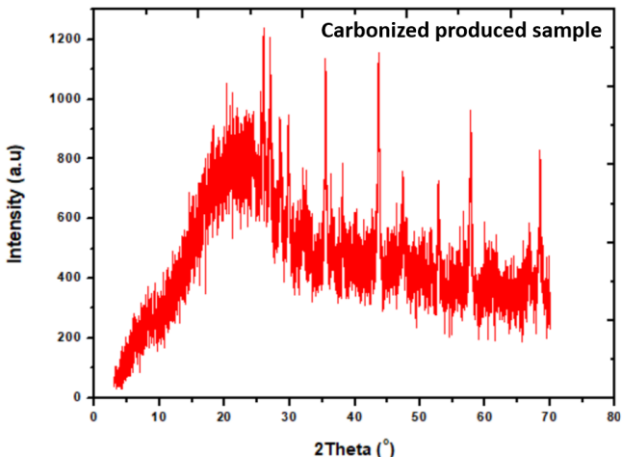

Figure 11. XRD spectrum of the carbonized bamboo culm-based composite sample

Figure 11 presents the XRD analysis of the carbonized bamboo culm-based composite sample. The XRD analysis of the carbonized bamboo sample revealed major peaks at 26°, 27°, 36°, 44°, 57°, and 69°, indicating a mix of graphitic and amorphous carbon phases [61, 62]. The dominant peak at 26° corresponds to the (002) plane of graphitic carbon, signifying partially ordered structures, while the peak at 27° suggests amorphous carbon contributions. The 36° and 44° peaks may indicate graphene nano-crystallites and the (100) plane of graphitic carbon, respectively, highlighting in-plane carbon ordering. The 57° and 69° peaks suggest higher-order reflections of turbostratic carbon, indicating stacked but disordered graphene layers. The high background noise confirms a significant amorphous content, which influences the material's mechanical strength, thermal stability, and wear resistance [27, 63]. These characteristics are critical for brake pad applications, as the presence of graphitic carbon enhances frictional performance, reduces wear, and improves heat dissipation, making carbonized bamboo a potential eco-friendly material for high-performance friction components [27, 42, 43, 61-63].

3.9 Scanning electron microscope (SEM) analysis

Figures 12(a-c) present the SEM micrographs of the produced composite samples. Evident in the SEM micrographs are uniform dark regions, which indicate the presence of graphite that was used to reduce wear in the composition, while the white regions indicate the presence of aluminum oxide which serves as an abrasive in the formulation. Also, the reinforcing material is seen at a mixed region of dark and white with the addition of iron filings that aided the composite sample's structural strength. The 30% resin aided the interfacial bonding of the produced sample. The SEM also shows a good combination of the element/oxide distribution in the formulation with a fair bonding of the resins and the bamboo culm particles. The XRF reveals the predominance of CaO (51.16%), SiO_2 (18.31%), and Cl (10.12%), as well as the presence of other elements/oxides (Figures 12(a-c)). In the composites, there have been visible fiber pull-out and tiny pores. According to Dagwa et al. [30] and Chaturvedi et al.

[64], the rough surface of the fiber of bamboo culm has stronger mechanical interactions with a matrix, leading to outstanding mechanical properties. Figure 12(d-f) presents the SEM micrographs of the commercial composite sample, which shows a more segmented, broken, and scattered orientation. The void spaces can be seen with some white dotted structures, which may indicate the presence of aluminum oxide. The XRF reveals the predominance of MgO (21.67%), CaO (19.27%), SiO_2 (17.16%), and Fe_2O_3 (15.98%) as well as the presence of other elements/oxides (Figure 11(d-f)). The compositions of SiO_2 (18.31%) and Al_2O_3 (3.14%) in the produced samples compare favorably with the compositions of SiO_2 (17.16%) and Al_2O_2 (4.57%) in the commercial sample. These findings agree with the works of other researchers [30, 64-67] on the mechanical and microstructural characterizations and fiber interactions with the matrix in the sample compositions.

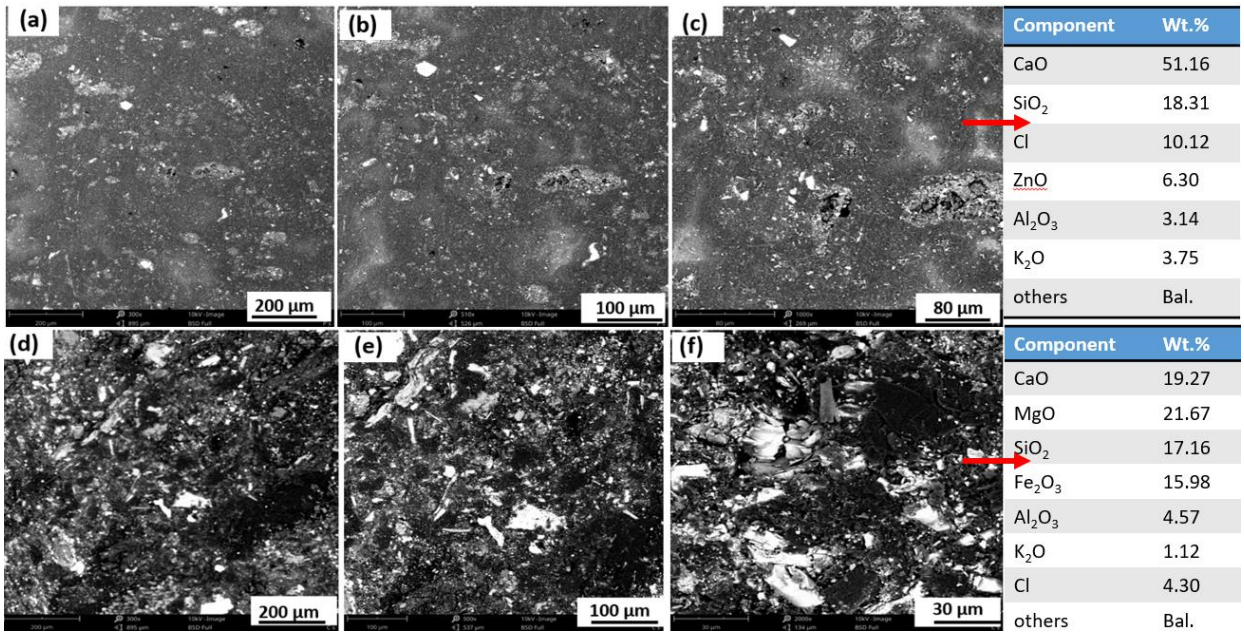

Component	Wt.%
CaO	51.16
SiO_2	18.31
Cl	10.12
ZnO	6.30
Al_2O_3	3.14
K_2O	3.75
others	Bal.

Component	Wt.%
CaO	19.27
MgO	21.67
SiO_2	17.16
Fe_2O_3	15.98
Al_2O_3	4.57
K_2O	1.12
Cl	4.30
others	Bal.

Figure 12. SEM micrographs of (a) produced composite sample (300x) with 30% resin, (b) produced composite sample (500x) with 30% resin, (c) produced composite sample (1000x) with 30% resin and XRF spectra results (d) commercial composite sample (300x) (e) commercial composite sample (500x) and (f) commercial composite sample (2000x), and XRF results

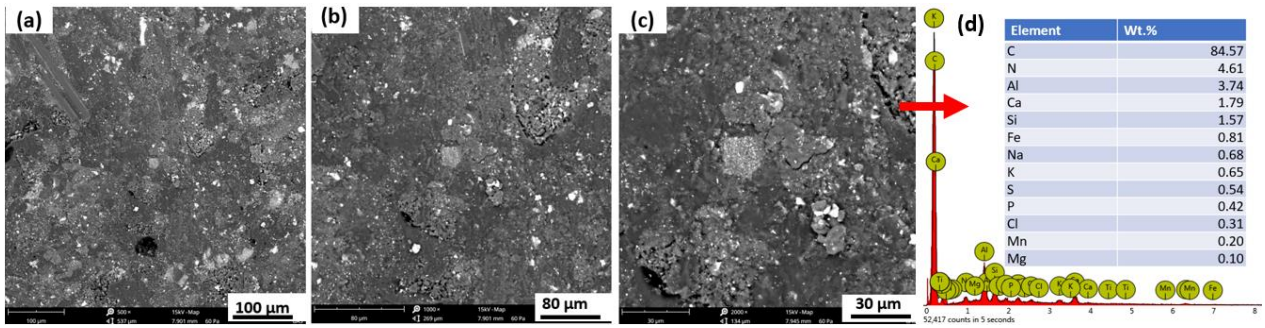

Element	Wt.%
C	84.57
N	4.61
Al	3.74
Ca	1.79
Si	1.57
Fe	0.81
Na	0.68
K	0.65
S	0.54
P	0.42
Cl	0.31
Mn	0.20
Mg	0.10

Figure 13. SEM micrographs of produced composite sample with 30% resin and magnifications of (a) 500x, (b) 1000x, (c) 2000x, and (d) EDS spectrum results

Figure 13(a-c) presents SEM micrographs of the worn surface of a carbonized bamboo culm-based composite material with 30% resin, captured at magnifications of 500×, 1000×, and 2000×, respectively, while Figure 13(d) displays the EDS spectrum results. The micrographs reveal a heterogeneous surface morphology exhibiting signs of abrasive wear, material pull-out, and surface fragmentation [62, 64]. The EDS analysis confirms a dominant carbon content (84.57 wt.%), which is critical for thermal stability and mechanical integrity in frictional applications, while the presence of Al, Ca, Si, and Fe suggests the formation of reinforcing compounds that enhance wear resistance [8, 55]. The observed wear mechanisms are predominantly abrasive and adhesive, as evidenced by micro-fractures and surface irregularities resulting from mechanical stresses during frictional contact. The high carbon composition contributes to self-lubricating properties, reducing the coefficient of friction and minimizing wear rates [62]. Additionally, the presence of silicate and oxide compounds associated with Si, Al, and Ca enhance the composite's ability to withstand extreme temperatures and wear conditions [64]. The existence of plowing grooves and asperities suggests material removal due to hard particle interactions, while wear debris formation during frictional engagement accelerates surface roughening [27]. The resin content plays a crucial role in maintaining structural cohesion, preventing excessive fragmentation, and improving wear resistance. These wear characteristics align with prior studies on biomass-derived composite materials,

further confirming the potential of carbonized bamboo culm composites for high-performance applications such as brake pads and other tribological components [8, 27, 52, 62, 64, 67, 68].

4. CONCLUSION

At the completion of this study, the following conclusions were reached:

i. With the use of an epoxy resin binder, cast-iron filings, graphite, and aluminum oxide in a variety of compositions, composite samples made from bamboo culm (*Bambusa vulgaris*) have been successfully developed.

ii. In comparison to uncarbonized *Bambusa vulgaris*, carbonized bamboo culm at 800°C with a carbonizing time of 64 minutes and a holding time of 1 hour had better physio-mechanical properties in terms of water and oil absorption, density, hardness, and coefficient of friction.

iii. Compared to the commercial sample's average hardness value of 71.87 HV, the carbonized composite sample's average hardness value of 107 HV provided the best surface hardness. This is because the bond interaction of epoxy, which keeps the components together, has led to an increase in its bonding materials.

iv. On the other hand, the tests' findings also show that the composite material developed has outstanding mechanical strength, with average values for its tensile strength, modulus of elasticity, and impact strength of 10.31 ± 0.21 MPa, 80.07 ± 1.60 MPa, and 0.6912 J/mm, respectively.

v. The resulting composite samples' coefficients of friction of 0.36, 0.39, and 0.38 compare favorably with the ranges of the generally accepted standard for automotive brake pad systems, which is between 0.3 and 0.45.

vi. When compared to commercial brake pads, the developed composite brake pads from bamboo culm's microstructure had a more uniform distribution of fillers, which improved bonding. Also, the compositions of SiO_2 (18.31%) and Al_2O_3 (3.14%) in the produced samples compare favorably with the compositions of SiO_2 (17.16%) and Al_2O_2 (4.57%) in the commercial sample from the XRF analysis.

vii. The SEM-EDS analysis of the worn sample clearly confirms the potential of carbonized bamboo culm-based composites for high-performance tribological applications, exhibiting outstanding wear resistance, thermal stability, and self-lubricating properties crucial for brake pads and friction materials.

The long-term durability and industrial feasibility of bamboo culm composites require attention. Challenges include moisture degradation, thermal instability, and bio-degradation. Industrial adoption faces raw material variability, machining difficulties, and cost concerns. Future research should optimize processing, enhance durability, and assess large-scale feasibility to ensure competitiveness with conventional brake pad materials in real-world applications.

ACKNOWLEDGMENTS

The management of the University of Abuja, Gwagwalada, Abuja, Nigeria, is appreciated by the authors for providing the TETFund IBR Grant (Award No. TETFund IBR-UARG/002) for this study.

REFERENCES

[1] Hentati, N., Makni, F., Elleuch, R. (2023). Braking performance of friction materials: A review of manufacturing process impact and future trends. Tribology-Materials, Surfaces & Interfaces, 17(2): 136-157. https://doi.org/10.1080/17515831.2023.2216092

[2] Ekpruke, E., Ossia, C.V., Big-Alabo, A. (2023). Recent progress and evolution in the development of non-asbestos based automotive brake pads-A review. Journal of Manufacturing Engineering, 18(2): 58-70. https://doi.org/10.37255/jme.v18i2pp058-070

[3] Li, G. (2018). The design of the automobile brake cooling system. Open Access Library Journal, 5(4): 1-10. https://doi.org/10.4236/oalib.1104567

[4] Dirisu, J.O., Okokpujie, I.P., Joseph, O.O., Oyedepo, S.O., Falodun, O., Tartibu, L.K., Shehu, F.D. (2024). Sustainable biocomposites materials for automotive brake pad application: An overview. Journal of Renewable Materials, 12(3): 485-511. http://doi.org/10.32604/jrm.2024.045188

[5] Lazarus, A.A., Philip, A. (2011). Asbestosis. Disease-a-Month, 57(1): 14-26. https://doi.org/10.1016/j.disamonth.2010.11.004

[6] Kishimoto, T., Morinaga, K., Kira, S. (2000). The prevalence of pleural plaques and/or pulmonary changes among construction workers in Okayama, Japan. American Journal of Industrial Medicine, 37(3): 291-295. https://doi.org/10.1002/(SICI)1097-0274(200003)37:3<291::AID-AJIM7>3.0.CO;2-A

[7] Ibhadode, A.A., Dagwa, I.M. (2008). Development of asbestos-free friction lining material from palm kernel shell. Journal of the Brazilian Society of Mechanical Sciences and Engineering, 30(2): 166-173. https://doi.org/10.1590/S1678-58782008000200010

[8] Abutu, J., Lawal, S.A., Ndaliman, M.B., Araga, R.L. (2018). An overview of brake pad production using non-hazardous reinforcement materials. Acta Technica Corviniensis-Bulletin of Engineering, 11(3): 143-156.

[9] Ghazali, C.M.R., Kamarudin, H., Jamaludin, S.B., Abdullah, M.M.A.B. (2011). Comparative study on thermal, compressive, and wear properties of palm slag brake pad composite with other fillers. Advanced Materials Research, 328-330: 1636-1641. https://doi.org/10.4028/www.scientific.net/AMR.328-330.1636

[10] Egeonu, D., Oluah, C., Okolo, P. (2015). Production of eco-friendly brake pad using raw materials sourced locally in Nsukka. Journal of Energy Technologies and Policy, 5(11): 47-54.

[11] Koya, O.A., Fono, T.R. (2009, February). Palm kernel shell in the manufacture of automotive brake pad. In International Seminar on Harnessing Natural Resources for National Development, Raw Materials Research & Development Council, pp. 10-13.

[12] Namessan, N.O., Maduako, J.N., Iya, S. (2012). Effect of

polyester and filler on water absorption behavior, density and porosity of kenaf (Hibiscus cannabinus) fibre reinforced brake pads. International Journal of Basic and Applied Sciences, 12(3).
[13] Aigbodion, V.S., Akadike, U., Hassan, S.B., Asuke, F., Agunsoye, J.O. (2010). Development of asbestos-free brake pad using bagasse. Tribology in Industry, 32(1): 12.
[14] Azeez, M.A., Orege, J.I. (2018). Bamboo, its chemical modification and products. Bamboo-current and Future Prospects, 25-48. https://doi.org/10.5772/intechopen.76359
[15] Sánchez Vivas, L. (2019). Bamboo as a Sustainable Engineering Material: Mechanical Properties, Safety Factors, and Experimental Testing. Practical Action Publishing.
[16] Ma, Y., Liu, Y., Tong, J. (2018). Bamboo wear and its application in friction material. Journal of Applied Polymer Science. https://doi.org/10.5772/intechopen.69893
[17] Irawan, A.P., Fitriyana, D.F., Tezara, C., Siregar, J.P., Laksmidewi, D., Baskara, G.D., Abdullah, M.Z., Junid, R., Hadi, A.E., Hamdan, M.H.M., Najid, N. (2022). Overview of the important factors influencing the performance of eco-friendly brake pads. Polymers, 14(6): 1180. https://doi.org/10.3390/polym14061180
[18] Borawski, A. (2020). Conventional and unconventional materials used in the production of brake pads-review. Science and Engineering of Composite Materials, 27(1): 374-396. https://doi.org/10.1515/secm-2020-0041
[19] Siregar, J.P., Rejab, M.R.M., Cionita, T., Hadi, A.E., Jaafar, J., Fitriyana, D.F., Dewi, R. (2024). Opportunities and challenges in the sustainable integration of natural fibers and particles in friction materials for eco-friendly brake pads. Mechanical Engineering for Society and Industry, 4(3): 337-367. https://doi.org/10.31603/mesi.12271
[20] Ammar, Z., Ibrahim, H., Adly, M., Sarris, I., Mehanny, S. (2023). Influence of natural fiber content on the frictional material of brake pads-A review. Journal of Composites Science, 7(2): 72. https://doi.org/10.3390/jcs7020072
[21] Kodric, M., Islam, M.R., Khatun, M.M., Motaleb, K.A. (2024). Thermoset and thermoplastic polymer composites reinforced with flax fiber: Properties and application-A review. SPE Polymers, 6(1): e10172. https://doi.org/10.1002/pls2.10172
[22] Kumar, N., Mehta, V., Kumar, S., Grewal, J.S., Ali, S. (2022). Bamboo natural fiber and PAN fiber used as a reinforced brake friction material: developed asbestos-free brake pads. Polymer Composites, 43(5): 2888-2895. https://doi.org/10.1002/pc.26584
[23] Lawal, S.S., Ademoh, N.A., Bala, K.C., Abdulrahman, A.S. (2019). A review of the compositions, processing, materials and properties of brake pad production. Journal of Physics: Conference Series, 1378(3): 032103. https://doi.org/10.1088/1742-6596/1378/3/032103
[24] Rao, R.U., Babji, G. (2015). A review paper on alternate materials for Asbestos brake pads and its characterization. International Research Journal of Engineering and Technology, 2(2): 556-562.
[25] Lobovikov, M., Ball, L., Guardia, M. (2007). World bamboo resources: A thematic study prepared in the framework of the global forest resources assessment 2005 (No. 18). Food & Agriculture Organization.
[26] Julong, D. (1989). Introduction to grey system theory. The Journal of Grey System, 1(1): 1-24.
[27] Lee, K., Ryu, S.K., Kim, H.G., Kwac, L.K., Kim, Y.S. (2024). Comparative analysis of graphitization characteristics in bamboo and oak charcoals for secondary battery anodes. Crystals, 14(11): 914. https://doi.org/10.3390/cryst14110914
[28] Subyakto, S., Budiman, I., Pari, G. (2012). Effects of temperature and time of carbonization on the properties of bamboo (Dendrocalamus asper) carbon. Wood Research Journal, 3(2): 68-73.
[29] Guo, H., Wang, F., Luo, H., Li, Y., Lou, Z., Ji, Y., Jiang, S. (2021). Flexible TaC/C electrospun non-woven fabrics with multiple spatial-scale conductive frameworks for efficient electromagnetic interference shielding. Composites Part A: Applied Science and Manufacturing, 151: 106662. https://doi.org/10.1016/j.compositesa.2021.106662
[30] Dagwa, I.M., Egege, C.M., Omiogbemi, I.M.B., Arogundade, A.I. (2021). Physical and thermo-mechanical behaviour of adansonia digitata-glass fibres and ceramic hybrid epoxy composite. Materials Today: Proceedings, 45: 4587-4594. https://doi.org/10.1016/j.matpr.2020.12.1230
[31] Adewumi, E., Mgbemena, C.O., Omiogbemi, I.M.B., Eguavoen, K.N., Dauda, D.W. (2020). Design and development of crash helmet from Musa-Paradisiaca's fibre as a reinforced composite. Materials Today: Proceedings, 21: 1566-1571. https://doi.org/10.1016/j.matpr.2019.11.091
[32] Yawas, D.S., Aku, S.Y., Amaren, S.G. (2013). Morphology and properties of periwinkle shell asbestos-free brake pad. Journal of King Saud University - Engineering Sciences, 28(1): 103-109. https://doi.org/10.1016/j.jksues.2013.11.002
[33] Edokpia, R.O., Aigbodion, V.S., Obiorah, O.B., Atuanya, C.U. (2014). Evaluation of the properties of ecofriendly brake pad using egg shell particles-gum Arabic. Results in Physics, 4: 68-77. https://doi.org/10.1016/j.rinp.2014.06.003
[34] Naik, S., Halemani, B., Raju, G.U. (2019). Investigation of the mechanical properties of tamarind seed particles reinforced epoxy composites. AIP Conference Proceedings, 2057(1): 1-8. https://doi.org/10.1063/1.5085594
[35] ASTM International. (2020). Standard test methods for density and specific gravity (relative density) of plastics by displacement (ASTM D792-20). American Society for Testing and Materials.
[36] Nishino, T., Hirao, K., Kotera, M., Nakamae, K., Inagaki, H. (2003). Kenaf reinforced biodegradable composites. Composites Science and Technology, 63(9): 1281-1286. https://doi.org/10.1016/S0266-3538(03)00099-X
[37] ASTM International. (2022). Standard test method for water absorption of plastics (ASTM D570-22). https://doi.org/10.1520/D0570-22
[38] Smales, H. (1995). Friction materials-Black art or science? Journal of Automobile Engineering, 209(D3): 151-157. https://doi.org/10.1243/PIME_PROC_1995_209_200_02
[39] Omiogbemi, I.M.B., Yawas, D.S., Dagwa, I.M., Okibe, F.G. (2017). Effects of metal inert gas welding parameters on some mechanical properties of austenitic

stainless steel in acidic environment. Nigerian Journal of Technology, 36(3): 835-843. http://doi.org/10.4314/njt.v36i3.25

[40] Omiogbemi, I.M.B., Yawas, D.S., Das, A., Afolayan, M.O., Dauda, E.T., Kumar, R., Gorja, S.R.S.R., Chowdhury, S.G. (2022). Mechanical properties and corrosion behaviour of duplex stainless steel weldment using novel electrodes. Scientific Reports, 12: 22405. https://doi.org/10.1038/s41598-022-26974-6

[41] Ademoh, N.A., Olabisi, A.I. (2015). Development and evaluation of maize husks (asbestos-free) based brake pad. Industrial Engineering Letters, 5(2): 67-80.

[42] Sá Ribeiro, R.A., Sá Ribeiro, M.G., Sankar, K., Kriven, W.M. (2016). Geopolymer-bamboo composite-A novel sustainable construction material. Construction and Building Materials, 123: 501-507. https://doi.org/10.1016/j.conbuildmat.2016.07.037

[43] Chin, S.C., Tee, K.F., Tong, F.S., Ong, H.R., Gimbun, J. (2020). Thermal and mechanical properties of bamboo fiber reinforced composites. Materials Today Communications, 23: 100876. https://doi.org/10.1016/j.mtcomm.2019.100876

[44] Omiogbemi, I.M.B., Yawas, D.S., Das, A., Afolayan, M.O., Dauda, E.T., Kumar, R., Gorja, S.R.S.R., Chowdhury, S.G. (2023). Effect of electrode configuration on the mechanical-corrosion characteristics of welded AISI 2205 steel structure. MRS Advances. https://doi.org/10.1557/s43580-022-00489-8

[45] Kumar, A. (2024). Microstructural evaluation of Al-Al_2O_3 composites processed by stir casting technique. Journal of Materials, 2(4): 267-272.

[46] Verma, S., Santra, B., Chattaraj, A., Samanta, A., Chowdhury, S., Srivastava, S., Sagdeo, A., Kanjilal, A., Katharria, Y.S. (2024). Two-step growth of alumina nanoparticle decorated graphene oxide surfaces: Effect on photocatalytic activity. Journal of Applied Physics, 135(6): 064901. https://doi.org/10.1063/5.0180885

[47] Wu, Y., Wang, Z., Zhang, R., Xin, G., Hu, H., Yan, X., Shi, X. (2024). A hermetic conformal coating based high-temperature encapsulation method for 250°C SiC power module. IEEE Transactions on Power Electronics, 40(3): 4090-4099. https://doi.org/10.1109/TPEL.2024.3492213

[48] Tao, F., Jiang, S., Feng, C. (2021). Research and design of dew point sensor based on α-Al_2O_3/SiO_2 composite dielectric material. In 2021 IEEE 5th Information Technology, Networking, Electronic and Automation Control Conference (ITNEC), Xi'an, China, pp. 1228-1231. https://doi.org/10.1109/ITNEC52019.2021.9587275

[49] Oh, E., Zúniga, M.M.G., Nguyen, T.B., Kim, B.H., Tien, T.T., Suhr, J. (2024). Sustainable green composite materials in the next-generation mobility industry: Review and prospective. Advanced Composite Materials, 33(6): 1368-1419. https://doi.org/10.1080/09243046.2024.2348237

[50] Moreno-Chocontá, L.N., Lozano-Pérez, A.S., Guerrero-Fajardo, C.A. (2024). Evaluation of the effect of particle size and biomass-to-water ratio on the hydrothermal carbonization of sugarcane bagasse. Chemical Engineering, 8(2): 43. https://doi.org/10.3390/chemengineering8020043

[51] Ali, A., Chhabra, D., Kumari, M., Manisha, M., Tiwari, P., Sahdev, R.K. (2024). Optimization and characterization of hybrid bio-briquettes produced from the mixture of sawdust, sugarcane bagasse, and paddy straw. Environmental Science and Pollution Research, 31(10): 15467-15490. https://doi.org/10.1007/s11356-024-32171-x

[52] Mohamed, Y.S., El-Gamala, H., Mahmoud, M., Zaghloul, Y. (2018). Micro-hardness behavior of fiber reinforced thermosetting composites embedded with cellulose nano-crystals. Alexandria Engineering Journal, 57(4): 4113-4119. https://doi.org/10.1016/j.aej.2018.10.012

[53] Abutu, J., Lawal, S.A., Ndaliman, M.B., Lafia-Araga, R.A., Adedipe, O., Choudhury, I.A. (2019). Production and characterization of brake pad developed from coconut shell reinforcement material using central composite design. SN Applied Sciences, 1: 82. https://doi.org/10.1007/s42452-018-0084-x

[54] Gai, P.F., Adisa, A.B., Aje, T., Bawa, M.A. (2022). Physico-mechanical properties of basalt-based brake pad as alternative to ceramics brake pad. Saudi Journal of Engineering and Technology, 7(1): 16-33. https://doi.org/10.36348/sjet.2022.v07i01.003

[55] Zhang, N., Jiang, G.J., Wu, D.W., Chen, H.X., Wu, J.X. (2021). Fatigue reliability analysis of the brake pads considering strength degradation. Eksploatacja i Niezawodność, 22(4): 620-626. http://doi.org/10.17531/ein.2020.4.5

[56] Synák, F., Jakubovičová, L., Klačko, M. (2022). Impact of the choice of available brake discs and brake pads at different prices on selected vehicle features. Applied Sciences, 12(14): 7325. https://doi.org/10.3390/app12147325

[57] Abutu, J., Lawal, S.A., Ndaliman, M.B., Lafia-Araga, R.A., Adedipe, O., Choudhury, I.A. (2018). Effects of process parameters on the properties of brake pad developed from seashell as reinforcement material using grey relational analysis. Engineering Science and Technology, an International Journal, 21(4): 787-797. https://doi.org/10.1016/j.jestch.2018.05.014

[58] Yao, F., Wu, Q., Lei, Y., Guo, W., Xu, Y. (2008). Thermal decomposition kinetics of natural fibers: Activation energy with dynamic thermogravimetric analysis. Polymer Degradation and Stability, 93(1): 90-98. https://doi.org/10.1016/j.polymdegradstab.2007.10.012

[59] Kozłowski, R., Przybylak, M.W. (2008). Flammability and fire resistance of composites reinforced by natural fibers: Review. Polymers for Advanced Technologies, 19(6): 446-453. https://doi.org/10.1002/pat.1135

[60] Dagwa, I.M., Ibhadode, A.O.A. (2005). Design and manufacture of automobile disk brake pad test rig. Nigerian Journal of Engineering Research and Development, 4(3): 15-24.

[61] Rajulu, A.V., Rao, G.B., Devi, L.G., Ramaiah, S., Prada, D.S., Bhat, K.S., Shyalashree, R. (2005). Mechanical properties of short, natural fiber Hildegardia populifolia-reinforced styrenated polyester composites. Journal of Reinforced Plastics and Composites, 24(4): 423-428. https://doi.org/10.1177/0731684405044896

[62] Li, Y., Jiang, L., Xiong, C., Peng, W. (2015). Effect of Different surface treatment for bamboo fiber on the crystallization behavior and mechanical property of bamboo fiber/nanohydroxyapatite/poly(lactic-co-glycolic) composite. Industrial & Engineering Chemistry Research, 54(48): 12017-12024.

https://doi.org/10.1021/acs.iecr.5b02724
[63] Ma, Y., Shen, S., Tong, J., Ye, W., Yang, Y., Zhou, J. (2013). Effects of bamboo fibers on friction performance of friction materials. Journal of Thermoplastic Composite Materials, 26(6): 845-859. https://doi.org/10.1177/0892705712461513
[64] Chaturvedi, K., Singhwane, A., Dhangar, M., Mili, M., Gorhae, N., Naik, A., Prashant, N., Srivastava, A.K., Verma, S. (2024). Bamboo for producing charcoal and biochar for versatile applications. Biomass Conversion and Biorefinery, 14(14): 15159-15185. https://doi.org/10.1007/s13399-022-03715-3
[65] Al-Shaabania, Y.A. (2019). Wear and Friction Properties of epoxy-polyamide blend nanocomposites reinforced by MWCNTs. Energy Procedia, 157: 1561-1567. https://doi.org/10.1016/j.egypro.2018.11.322
[66] Osorio, L., Trujillo, E., Lens, F., Ivens, J., Verpoest, I., Van Vuure, A.W. (2018). In-depth study of the microstructure of bamboo fibres and their relation to the mechanical properties. Journal of Reinforced Plastics and Composites, 37(17): 1099-1113. https://doi.org/10.1177/0731684418783055
[67] Malekzadeh, H., Md Zaid, N.S.B., Bele, E. (2021). Characterization and structural properties of bamboo fibre solid foams. Cellulose, 28(1): 703-714. https://doi.org/10.1007/s10570-020-03565-0
[68] Lee, H.S., Purusatama, B.D., Febrianto, F., Lee, S.H., Kim, N.H. (2023). Morphological, physical, chemical, and thermal decomposition properties of air-heat-treated balsa fruit fibers at different temperatures. Cellulose, 30(13): 8369-8385. https://doi.org/10.1007/s10570-023-05390-7